

# Modeling complex crack problems using the numerical manifold method

G. W. Ma · X. M. An · H. H. Zhang · L. X. Li

Received: 9 October 2008 / Accepted: 6 April 2009 / Published online: 28 April 2009  
© Springer Science+Business Media B.V. 2009

**Abstract** In the numerical manifold method, there are two kinds of covers, namely mathematical cover and physical cover. Mathematical covers are independent of the physical domain of the problem, over which weight functions are defined. Physical covers are the intersection of the mathematical covers and the physical domain, over which cover functions with unknowns to be determined are defined. With these two kinds of covers, the method is quite suitable for modeling discontinuous problems. In this paper, complex crack problems such as multiple branched and intersecting cracks are studied to exhibit the advantageous features of the numerical manifold method. Complex displacement discontinuities across crack surfaces are modeled by different cover functions in a natural and straightforward manner. For the crack tip singularity, the asymptotic near tip field is incorporated to the cover function of the singular physical cover. By virtue of the domain form of the interaction integral, the mixed mode stress intensity factors are evaluated for three typical examples. The excellent results show that the numerical manifold method is prominent in modeling the complex crack problems.

**Keywords** Numerical manifold method · Mathematical cover · Physical cover · Weight function · Cover function · Complex crack problems

## 1 Introduction

Modeling complex crack problems is highly important for researchers and engineers to quantitatively predict the life span of cracked structures under service conditions (Daux et al. 2000). For this purpose, a number of numerical approaches have been proposed in the past several decades. Through embedding the singular elements at crack tips, the finite element method (FEM) was successfully used to compute the stress intensity factor (SIF) (Barsoum 1977; Kwon and Akin 1989). However, as we know, in this kind of method, the crack geometries must be considered at the stage of mesh generation. This leads to prohibitive burden in meshing or remeshing for the complex crack problems, such as multiple cracks, intersecting cracks, branched cracks, and their growth (Karihaloo and Xiao 2003).

Another effective approach to model crack problems is the use of meshless (or element-free) methods. Since elements are not involved any more, meshless methods avoid distortion or coincidence of elements with the crack geometries, and therefore are regarded as being more effective than the FEM in this respect (Belytschko et al. 1996; Rao and Rahman 2000; Dufloot and Nauyen-Dang 2004). In particular, in the element-free Galerkin (EFG) method, as a representative, introduction of the

---

G. W. Ma (✉) · X. M. An · H. H. Zhang · L. X. Li  
School of Civil and Environmental Engineering, Nanyang Technological University, Singapore 639798, Singapore  
e-mail: cgwma@ntu.edu.sg

H. H. Zhang · L. X. Li  
MOE Key Laboratory for Strength and Vibration, Xi'an Jiaotong University, 710049 Xi'an, Shaanxi, People's Republic of China

moving least squares in the interpolation approximation is beneficial to evaluate the SIF and to model the crack growth (Belytschko et al. 1994, 1995a,b, 1996; Krysl and Belytschko 1999; Muravin and Turkel 2006). However, as we know, the difficulties in the numerical integration and superimposition of essential boundary conditions are unavoidably encountered in this kind of methods (Strouboulis et al. 2000a,b).

At present, a great number of commercial computer codes have been developed by using the FEM. They are robust and versatile, owing to the advantageous features of the FEM. Within the same framework as the partition of unity method (PUM) (Melenk and Babuska 1996; Babuska and Melenk 1997), the extended finite element method (XFEM) (Daux et al. 2000; Moes et al. 1999; Sukumar and Prevost 2003; Huang et al. 2003; Sukumar et al. 2000) and the generalized finite element method (GFEM) (Strouboulis et al. 2000a,b, 2001) were proposed to overcome the difficulty of the FEM in mesh generation when tackling complex problems by constructing a desired conforming approximation space with a local property.

In the XFEM (Daux et al. 2000; Moes et al. 1999; Sukumar and Prevost 2003; Huang et al. 2003; Sukumar et al. 2000), a standard finite element mesh is first generated as if other internal entities were absent. Then, these discontinuities will be treated by enriching the interpolation approximation. Taking the crack problem as an example, the enrichments are two-folded in the XFEM. For the nodes whose support intersects the crack surface, they will be enriched with a generalized Heaviside function. For the nodes whose support contains the crack tip, they will be enriched with the asymptotic near tip field. In the GFEM (Strouboulis et al. 2000a,b, 2001), on the other hand, much attention has been paid to augmenting the finite element space with the analytically or numerically generated solution for a given problem on a coarse (or practically acceptable) but regular mesh. This method has been successfully used to tackle some typical problems with multiple reentrant corners, voids and cracks. In the GFEM, the integration is carried out by employing an effective jagged refinement algorithm even in an element with a very complex shape.

The numerical manifold method (NMM) (Shi 1991, 1992) originated from the topological manifold and differential manifold. Due to the partition of unity of the weight functions, the NMM can also be regarded as an extension of the FEM, like the XFEM and the GFEM.

More importantly, due to the cover-based property, the NMM is in essence different from the FEM, and particularly suitable for modeling discontinuous problems. The distinct features of the NMM can be manifested in two aspects. First, the mathematical covers in the NMM need not conform to the physical domain. Second, the degrees of freedom (DOFs) are associated with the physical covers, rather than the nodes, and therefore, discontinuities can be modeled in a more natural manner, even for a complex case.

The advantages of the NMM lie in solving discontinuous problems, and simple crack problems have been modeled by Tsay et al. (1999), Chiou et al. (2002) and Li et al. (2005). This paper intends to exhibit the capability of the NMM in modeling complex crack problems such as multiple intersecting cracks and branched cracks, as compared with other effective methods such as the XFEM and the GFEM. In Sect. 2, the NMM is systematically introduced in theory and implementation for complex crack problems. In Sect. 3, three numerical experiments are carried out, and the SIF results are compared with the available reference solutions. The conclusions from the current work are made finally in Sect. 4.

## 2 Modeling crack problems with the NMM

### 2.1 Fundamentals of the NMM

The NMM is based on three important concepts, i.e., mathematical cover (MC), physical cover (PC) and cover-based element (CE). MCs are user-defined overlapping small patches. Their union is independent of, but must cover the physical domain of the problem. PCs are the intersection of MCs and the physical domain. Here, we use physical domain to represent the portrait of a physical problem in a general sense. It includes the problem domain in which the physical problem is defined, and all the physical features such as internal discontinuities (e.g. joints, material interfaces and cracks) and external geometries on which boundary conditions are prescribed. Obviously, the physical domain is problem dependent. Thus, PCs are in fact the subdivision of MCs by the physical domain. Further, the CE in the NMM is defined as the common region of several PCs.

To visualize the three concepts, the example illustrated in Fig. 1 is used. There are two MCs in total, a

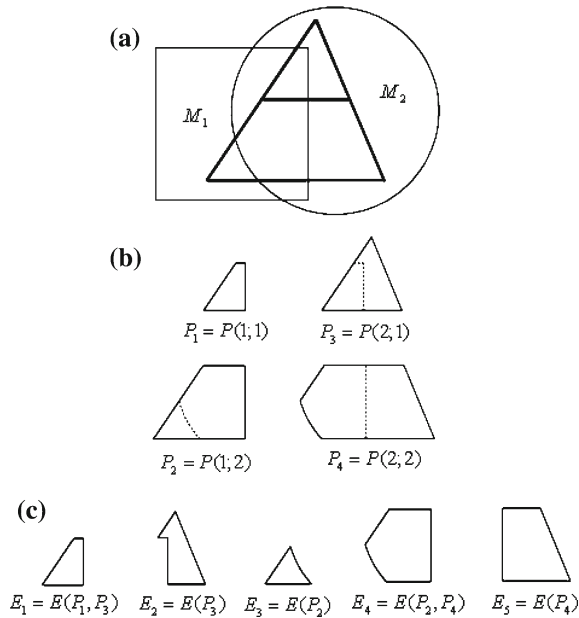


**Fig. 1** Covers and elements in the NMM. **a** The physical domain (circumscribed by the *thick lines*) and two mathematical covers. **b** Four corresponding physical covers. **c** Five corresponding cover-based elements

rectangle  $M_1$  and a circle  $M_2$ . The thick lines define the physical domain  $\Omega$ . Intersected with the physical domain,  $M_1$  and  $M_2$  are divided, respectively, into two PCs, i.e.  $P(1; 1)$  and  $P(1; 2)$ , and  $P(2; 1)$  and  $P(2; 2)$ , as shown in Fig. 1b. Here, notation  $P(i; j)$  represents the  $j$ th PC generated from the  $i$ th MC.

So far, each MC is associated with several PCs, and each PC has two indices, i.e.  $i$  and  $j$ . To simplify an implementation, it is helpful to reallocate a single index to each PC. Considering the simple example shown in Fig. 1, for instance, the four PCs can be renumbered by  $P_1 = P(1; 1)$ ,  $P_2 = P(1; 2)$ ,  $P_3 = P(2; 1)$ ,  $P_4 = P(2; 2)$  in light of different MCs.

These four PCs finally form five CEs as shown in Fig. 1c, numbered by  $E_1 = E(P_1, P_3)$ ,  $E_2 = E(P_3)$ , and so on.

On each MC  $M_I$ , a weight function is defined, which satisfies

$$\begin{aligned} \varphi_I(\mathbf{x}) &\in C^0(M_I) \\ \varphi_I(\mathbf{x}) &= 0, \mathbf{x} \notin M_I \end{aligned} \tag{1a}$$

with

$$\sum_{\substack{J \\ \text{if } \mathbf{x} \in M_J}} \varphi_J(\mathbf{x}) = 1 \tag{1b}$$

Equation 1a indicates that the weight function has non-zero value only on its corresponding MC, but zero otherwise, whereas Eq. 1b is just the partition of unity property to assure a conforming approximation. The weight function  $\varphi_I(\mathbf{x})$  associated with  $M_I$  will be accordingly transferred to  $P_i$ , any of the PCs  $P(I, j)$  in  $M_I$ , which is expressed as  $\varphi_i(\mathbf{x})$  on  $P_i$  hereafter.

With these concepts, the interpolation approximation can be constructed. First, a cover function  $\mathbf{u}_i(\mathbf{x})$  is defined individually as a local approximation on the PC  $P_i$  for the displacement field, which can be constant, linear, high order polynomials or other functions with unknowns (also termed DOFs) to be determined. Then, the global displacement  $\mathbf{u}(\mathbf{x})$  on a certain CE  $e$  is approximated to be

$$\mathbf{u}^h(\mathbf{x}) = \sum_{\substack{i \\ \text{if } e \subset P_i}} \varphi_i(\mathbf{x}) \cdot \mathbf{u}_i(\mathbf{x}) \tag{2}$$

### 2.2 Generation of physical covers for crack problems

In Fig. 1, we use rectangular and/or circular MCs. Theoretically, any shape of MCs can be accepted in the NMM. In this paper, for convenience of generating physical covers and constructing weight functions, a finite element mesh is adopted. To this end, the finite element mesh is re-examined from the viewpoint of the NMM. It is noted that the so-called finite element mesh here is independent of the physical domain of the problem, and therefore different from the one actually used in the FEM. Further, due to the dissimilarity between the physical domain and the union of MCs, the CEs may have arbitrary shape, different from the finite elements in the FEM, according to the formation procedure in the NMM.

Regarding the point at which the weight function is unity and in the neighborhood of which the weight function is not identically equal to unity as a star, the union of the finite elements sharing a same star forms a MC. Figure 2 shows a triangular finite element mesh, and a resulting hexagonal MC with the star marked by  $S$ . The weight function for such a hexagonal cover is easily constructed by borrowing the shape functions of the triangular finite element, and depicted in Fig. 3. It is not difficult to verify that the weight functions satisfy Eq. 1.

In the NMM, the MCs are designated by users, regardless of the crack entity. When a crack is present in

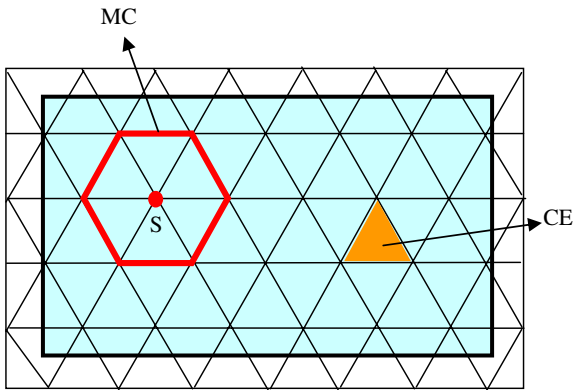


**Fig. 2** A triangular finite element mesh and the resulting MC

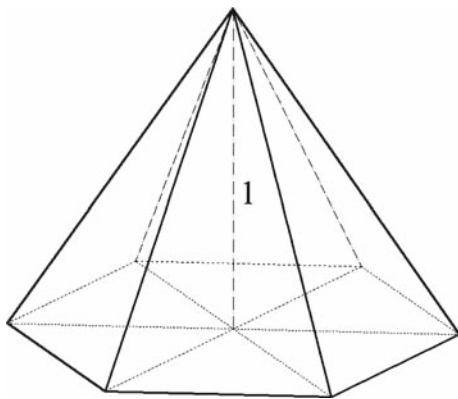


**Fig. 3** Weight function for a hexagonal MC

the physical domain, it will intersect some of the MCs (Lin 2003). As shown in Fig. 4a, for the MC split completely by a single crack surface, two different PCs will then be formed. Similarly, the MC split by a branched crack will become three PCs (Fig. 4b) while the MC split by an intersecting crack will generate four PCs (Fig. 4c). In the framework of the NMM, presence of a crack surface will produce additional PCs (Chen et al. 1998), and in general, if a MC is divided into  $m$  completely isolated regions by crack surfaces,  $m-1$  PCs will be added.

For the MC partially cut by the crack (shown in Fig. 4d), only one PC will be formed. This PC contains the crack tip singularity, and is called singular PC in this context, in contrast to other conventional PCs.

Hence, as shown in Fig. 5, when complex cracks are modeled with the NMM, each MC starred by square is divided into several conventional PCs, and each MC starred by circle becomes a single singular PC.

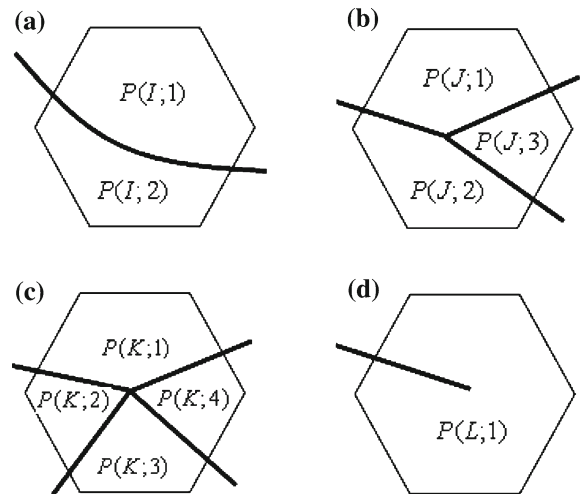


**Fig. 4** Generation of PCs for crack problems

### 2.3 Modeling cracks in the NMM

#### 2.3.1 Modeling displacement discontinuity across the crack surface

For the case of continuous problem, the displacement approximation in Eq. 2 is always continuous. For the case of discontinuous problem, as mentioned in Sect. 2.2, a crack surface may cut a MC into two conventional PCs. For clarity, we study the displacement along the crack surface while the crack passes through the shaded triangle shown in Fig. 6a. The triangle is formed by three MCs of  $M_5$ ,  $M_6$  and  $M_9$ . As shown in Fig. 6b,  $M_5$ ,  $M_6$  and  $M_9$  are divided, respectively, into two PCs, i.e.  $P(5; 1)$  and  $P(5; 2)$ ,  $P(6; 1)$  and  $P(6; 2)$ , and  $P(9; 1)$  and  $P(9; 2)$ . For convenience, the six PCs are renumbered by  $P_5 = P(5; 1)$ ,  $P_6 = P(5; 2)$ ,  $P_7 = P(6; 1)$ ,  $P_8 = P(6; 2)$ ,  $P_9 = P(9; 1)$ ,  $P_{10} = P(9; 2)$  in light of different MCs. Thus, from Eq. 2, the displacement jump across the crack surface in the shaded triangle is obtained as

$$\llbracket \mathbf{u}^h(\mathbf{x}) \rrbracket = \sum_{i \in \{5,7,9\}} \varphi_i(\mathbf{x}) \mathbf{u}_i - \sum_{i \in \{6,8,10\}} \varphi_i(\mathbf{x}) \mathbf{u}_i \quad (3)$$

Knowing that  $\varphi_5(\mathbf{x})$  and  $\varphi_6(\mathbf{x})$ ,  $\varphi_7(\mathbf{x})$  and  $\varphi_8(\mathbf{x})$ ,  $\varphi_9(\mathbf{x})$  and  $\varphi_{10}(\mathbf{x})$  are identical since they are defined on the same MC, the above equation can be further simplified as

**Fig. 5** Treatment of complex cracks in the NMM

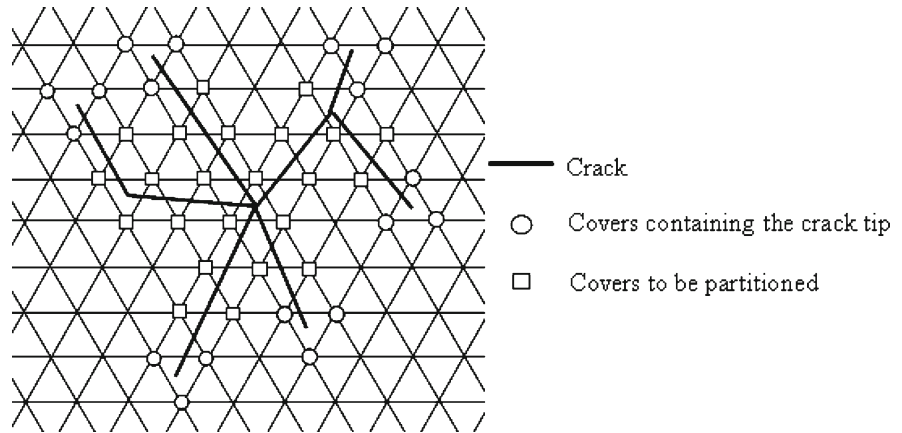
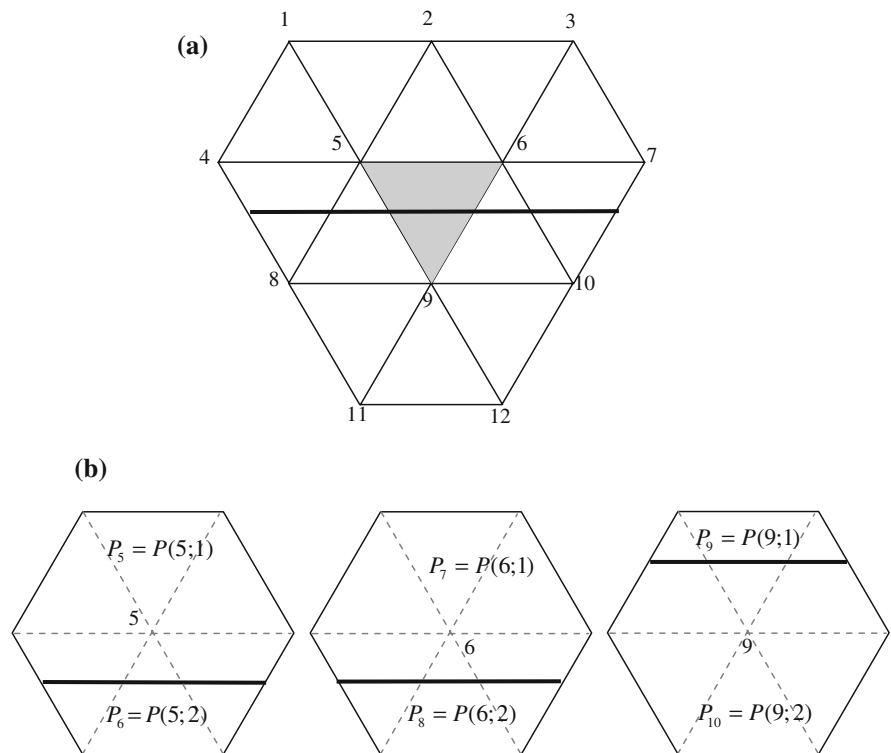


**Fig. 6** Illustration of modeling a crack surface with the NMM. **a** MC system. **b** PCs



$$\begin{aligned} \llbracket \mathbf{u}^h(\mathbf{x}) \rrbracket &= \varphi_5(\mathbf{x}) (\mathbf{u}_5 - \mathbf{u}_6) + \varphi_7(\mathbf{x}) (\mathbf{u}_7 - \mathbf{u}_8) \\ &\quad + \varphi_9(\mathbf{x}) (\mathbf{u}_9 - \mathbf{u}_{10}) \end{aligned} \tag{4}$$

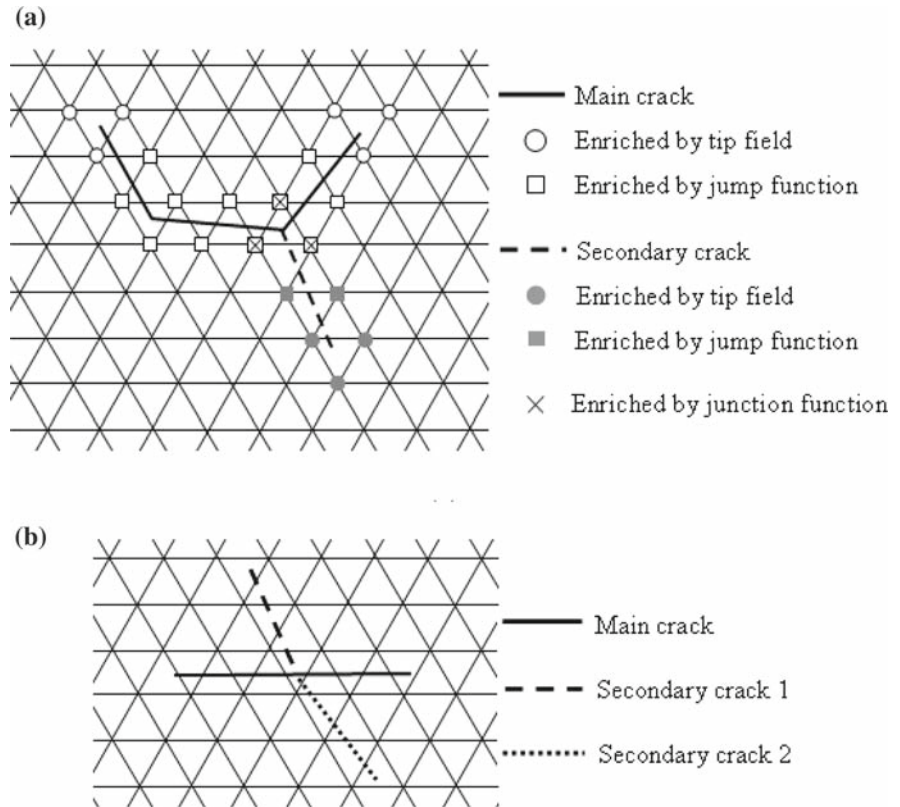
Considering that  $\mathbf{u}_5$  and  $\mathbf{u}_6$ ,  $\mathbf{u}_7$  and  $\mathbf{u}_8$ ,  $\mathbf{u}_9$  and  $\mathbf{u}_{10}$  are individually defined cover functions and contain independent DOFs, the displacement discontinuity can be obviously manifested.

Complex crack surfaces may cut the mathematical cover into more conventional PCs (e.g. three PCs for a branched crack, four PCs for an intersecting crack), as shown in Fig. 4a–c. Since there are independent cover

functions for each individual PC, the displacement discontinuity across any surface of multiple intersecting or branching crack surfaces will be modeled in a similar way, as indicated in Eq. 3.

Here, we compare the NMM with the XFEM and the GFEM in this respect. The XFEM adopts the generalized Heaviside function  $H(\mathbf{x})$  to describe the displacement discontinuity across a crack surface. The  $H(\mathbf{x})$  has two values, i.e., +1 above the crack surface and -1 below the crack surface. This function is valid to represent the displacement jump across a single crack

**Fig. 7** Treatment of complex cracks in the XFEM. **a** A branched crack. **b** An intersecting crack



surface. However, it is insufficient for complex crack problems. In such a case, additional technique must be adopted. For instance, in [Daux et al. \(2000\)](#), a branched crack is defined as the intersection of a main crack and a secondary crack (see Fig. 7a). First, the main crack is treated, in which the nodes whose support completely cut by the main crack surface are enriched with generalized Heaviside function and the nodes whose support containing the main crack tips with crack tip functions. Then the secondary crack is treated in a similar way. Lastly, a junction function  $J(\mathbf{x})$  is added to all the nodes whose support contains the junction. For an intersecting crack, a main crack and two secondary cracks (Fig. 7b) must be defined and then enriched accordingly. So, in the XFEM, enrichment for complex cracks are problem-dependent and requires additional functions. Recently, [Simone et al. \(2006\)](#) uses the GFEM for polycrystal by incorporating a different discontinuous function  $H_\alpha(\mathbf{x})$ , defined by  $H_\alpha(\mathbf{x}) = 1$  when  $\mathbf{x}$  within grain  $\zeta_\alpha$ , and 0 otherwise. Modeling a triple junction with this method is illustrated in Fig. 8. Later, [Duarte et al. \(2007\)](#) extended it for branched crack problems. This method is over the XFEM because

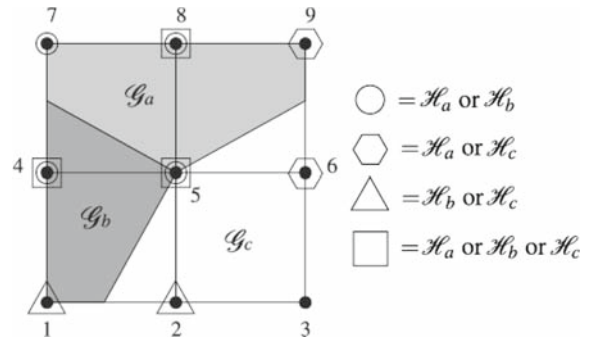


**Fig. 8** Treatment of a triple junction in the GFEM from [Simone et al. \(2006\)](#)

of its simplicity for arbitrary number of branches, selection of enrichment functions, and extension to three-dimensions. However, the discontinuous function in the GFEM is based on a polycrystalline aggregate topology, which only allows the crack to stop at the edge of finite elements.

To sum up, since the FEM was originally devised for continua, the displacement discontinuity can only be modeled by introducing additional functions in the



XFEM and the GFEM. In contrast, since the NMM was originally devised for discontinuous problems, even with movement, this discontinuity can be modeled in a straightforward and natural manner wherever the crack stops, even for complex cases (see Sect. 3.3), simply by using different cover functions associated with individual PCs inside one MC, without introducing any additional functions. This way can also be easily extended to the three-dimensional counterpart.

### 2.3.2 Modeling the near tip singularity in the NMM

The original NMM adopts a polynomial cover function. This is sufficient for conventional PCs, even to model the discontinuity across a crack surface. However, for a singular PC discussed in Sect. 2.2, because of the stress singularity near the crack tip, the polynomial cover function is insufficient. Considering the fact that the singular PC is formed by a whole MC, under which the NMM is identically reduced to the FEM in this case, a similar way suggested in the EFG (Fleming et al. 1997) and the XFEM (Moes et al. 1999; Daux et al. 2000) is chosen to enrich the cover functions as the local approximation on the same mathematical basis.

Thus, for a more general CE  $e$  with singular PCs, the global displacement approximation in Eq. 2 is rewritten as

$$\mathbf{u}^h(\mathbf{x}) = \sum_{i \in e \subset P_i} \varphi_i(\mathbf{x}) \cdot (\mathbf{u}_i(\mathbf{x}) + \hat{\mathbf{u}}_i(\mathbf{x})) \tag{5}$$

where  $\hat{\mathbf{u}}_i$  is an additional cover function for the  $i$ th PC.

The conventional cover function  $\mathbf{u}_i(\mathbf{x})$  is often expressed by

$$\mathbf{u}_i(\mathbf{x}) = \mathbf{p}^T(x) \cdot \mathbf{a}_i \tag{6}$$

where  $\mathbf{a}_i$  is the array of DOFs, and  $\mathbf{p}^T(\mathbf{x})$  is the matrix of polynomial bases as

$$\mathbf{p}^T(\mathbf{x}) = \begin{bmatrix} 1 & 0 & x & 0 & y & 0 & \dots \\ 0 & 1 & 0 & x & 0 & y & \dots \end{bmatrix} \tag{7}$$

in the two dimensional setting.

As we know, near the crack tip, the asymptotic two-dimensional field can be expanded by following four basis functions in isotropic elasticity (Fleming et al. 1997; Moes et al. 1999)

$$[\Phi_1 \ \Phi_2 \ \Phi_3 \ \Phi_4] = \left[ \sqrt{r} \sin \frac{\theta}{2}, \sqrt{r} \cos \frac{\theta}{2}, \sqrt{r} \sin \theta \sin \frac{\theta}{2}, \sqrt{r} \sin \theta \cos \frac{\theta}{2} \right] \tag{8}$$

where  $r$  and  $\theta$  are polar coordinates in the local crack tip coordinate system. It is noted that the four basis functions can construct arbitrary displacement field near the crack tip, and moreover, the first term which is discontinuous across the crack surface (i.e.  $\theta = \pm\pi$ ) will recover the jump property expressed in Eq. 3. Based on Eq. 8, the additional cover function for a singular cover takes the form

$$\hat{\mathbf{u}}_i = \Phi \mathbf{c}_i \tag{9}$$

where  $\mathbf{c}_i$  is the array of additional DOFs associated with the enrichment, and  $\Phi$  is the matrix of corresponding bases as

$$\Phi = \begin{bmatrix} \Phi_1 & 0 & \Phi_2 & 0 & \Phi_3 & 0 & \Phi_4 & 0 \\ 0 & \Phi_1 & 0 & \Phi_2 & 0 & \Phi_3 & 0 & \Phi_4 \end{bmatrix} \tag{10}$$

in the two-dimensional setting.

### 2.4 Formulations of the NMM

Discrete equations for a linear elastic problem with cracks can be obtained from the Galerkin formulation (Lin 2003). Let  $\mathbf{u} \in V$  be the displacement trial function with  $V = H^1(\Omega)$ , and  $\delta \mathbf{u} \in V$  be a test function. A weak form of the discrete problem on a CE  $e$  is to find  $\mathbf{u}^h$  in the finite dimensional subspace  $V^h \subset V$ ,  $\forall \delta \mathbf{u}^h \in V^h$ , such that

$$\begin{aligned} & \int_{\Omega_e} \boldsymbol{\sigma}(\mathbf{u}^h) : \boldsymbol{\varepsilon}(\delta \mathbf{u}^h) d\Omega + \lambda \int_{\Gamma_u^e} (\mathbf{u}^h - \bar{\mathbf{u}}) \cdot \delta \mathbf{u}^h d\Gamma \\ & = \int_{\Gamma_t^e} \bar{\mathbf{t}} \cdot \delta \mathbf{u}^h d\Gamma + \int_{\Omega_e} \mathbf{b} \cdot \delta \mathbf{u}^h d\Omega \end{aligned} \tag{11}$$

where  $\boldsymbol{\sigma}$  and  $\boldsymbol{\varepsilon}$  are stress tensor and strain tensor, respectively.  $\Omega_e$  is the domain occupied by the CE  $e$  subjected to the body force  $\mathbf{b}$ . The boundary conditions consist of the essential boundary condition  $\mathbf{u} = \bar{\mathbf{u}}$  on  $\Gamma_u^e$  and traction boundary condition  $\boldsymbol{\sigma} \cdot \mathbf{n} = \bar{\mathbf{t}}$  on  $\Gamma_t^e$ .

In the NMM, when tackling the discontinuities effectively, the essential boundary conditions are superimposed in a weak form, unlike in the FEM. This is because the union of MCs is not necessarily identical to the physical domain. In this paper, for the purpose of simplicity, the penalty method with a real penalty number  $\lambda$  is chosen to superimpose the essential boundary conditions, as the second term on the left hand in Eq. 11. Since the single-field formulations are preserved and no additional DOFs involved, the additional burden proves to be trivial by our numerical experiments.

From Eqs. 5 and 9, the trial function  $\mathbf{u}^h$  and the test function  $\delta\mathbf{u}^h$  are expressed as

$$\mathbf{u}^h(\mathbf{x}) = \sum \varphi_i(\mathbf{x}) \cdot (\mathbf{p}^T(\mathbf{x}) \cdot \mathbf{a}_i + \Phi \mathbf{c}_i) \tag{12a}$$

$$\delta\mathbf{u}^h(\mathbf{x}) = \sum \varphi_i(\mathbf{x}) \cdot (\mathbf{p}^T(\mathbf{x}) \cdot \delta\mathbf{a}_i + \Phi \delta\mathbf{c}_i) \tag{12b}$$

By substituting the above two equations into Eq. 11, and considering the arbitrariness of the test functions, we formally obtain

$$\mathbf{K}\mathbf{q} = \mathbf{F} \tag{13}$$

where  $\mathbf{q}$  is the vector of DOFs,  $\mathbf{K}$  and  $\mathbf{F}$  are the equivalent stiffness matrix and the load vector, respectively. The element contribution to  $\mathbf{K}$  and  $\mathbf{F}$  are as follows

$$\mathbf{k}_{ij}^e = \begin{bmatrix} \mathbf{k}^{\mathbf{a}_i \mathbf{a}_j} & \mathbf{k}^{\mathbf{a}_i \mathbf{c}_j} \\ \mathbf{k}^{\mathbf{c}_i \mathbf{a}_j} & \mathbf{k}^{\mathbf{c}_i \mathbf{c}_j} \end{bmatrix}, \tag{14a}$$

$$\mathbf{f}_i^e = \{ \mathbf{f}^{\mathbf{a}_i} \ \mathbf{f}^{\mathbf{c}_i} \}^T \tag{14b}$$

with their entries being

$$\mathbf{k}^{r_i s_j} = \int_{\Omega^e} (\mathbf{B}^{r_i})^T \mathbf{D} \mathbf{B}^{s_j} d\Omega + \lambda \int_{\Gamma_u^e} (\varphi_i \mathbf{P})^T \cdot (\varphi_j \mathbf{P}) d\Gamma(r_i, s_i = \mathbf{a}_i, \mathbf{c}_i) \tag{15a}$$

$$\mathbf{f}^{\mathbf{a}_i} = \int_{\Gamma_f^e} \varphi_i \mathbf{P} \bar{\mathbf{t}} d\Gamma + \int_{\Omega^e} \varphi_i \mathbf{P} \mathbf{b} d\Omega + \lambda \int_{\Gamma_u^e} \varphi_i \mathbf{P} \bar{\mathbf{u}} d\Gamma \tag{15b}$$

$$\mathbf{f}^{\mathbf{c}_i} = \int_{\Gamma_f^e} \varphi_i \Phi \bar{\mathbf{t}} d\Gamma + \int_{\Omega^e} \varphi_i \Phi \mathbf{b} d\Omega + \lambda \int_{\Gamma_u^e} \varphi_i \Phi \bar{\mathbf{u}} d\Gamma \tag{15c}$$

where  $\mathbf{D}$  is the elasticity matrix. The entries of the strain-displacement matrix  $\mathbf{B}$  are

$$\mathbf{B}^{\mathbf{a}_i} = \begin{bmatrix} (\varphi_i \mathbf{P})_{,x} & 0 \\ 0 & (\varphi_i \mathbf{P})_{,y} \\ (\varphi_i \mathbf{P})_{,y} & (\varphi_i \mathbf{P})_{,x} \end{bmatrix}, \tag{16a}$$

$$\mathbf{B}^{\mathbf{c}_i} = [\mathbf{B}_1 \ \mathbf{B}_2 \ \mathbf{B}_3 \ \mathbf{B}_4], \tag{16b}$$

$$\mathbf{B}_\alpha = \begin{bmatrix} (\varphi_i \Phi_\alpha)_{,x} & 0 \\ 0 & (\varphi_i \Phi_\alpha)_{,y} \\ (\varphi_i \Phi_\alpha)_{,y} & (\varphi_i \Phi_\alpha)_{,x} \end{bmatrix} \ (\alpha = 1 \sim 4). \tag{16c}$$

### 3 Numerical examples and discussion

In this section, we give three examples of complex crack problems by using the present NMM. In Sect. 3.1, a symmetrically branched crack problem is studied. In Sects. 3.2 and 3.3, problems with a star-shaped

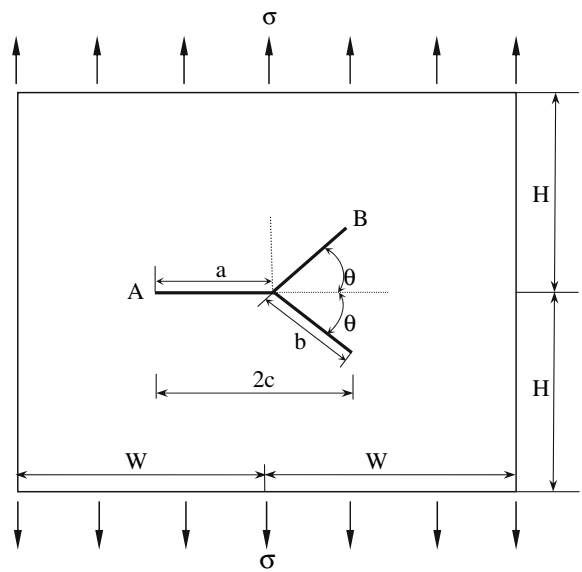


**Fig. 9** A symmetrically branched crack in a finite plate under tension

crack and a tree-shaped crack are investigated, respectively. For these crack problems, the SIFs are calculated through the domain form of interaction integral (Moes et al. 1999). For the SIF results, the convergence is studied, and the accuracy is compared with the reference solutions available.

#### 3.1 A symmetrically branched crack in a finite plate

Our numerical experiments start with a finite plate with a symmetrically branched crack under uniform tension as shown in Fig. 9.

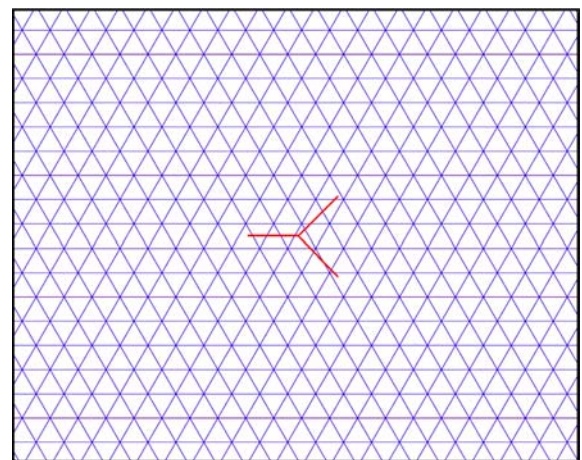


**Fig. 10** The branched crack and the MCs



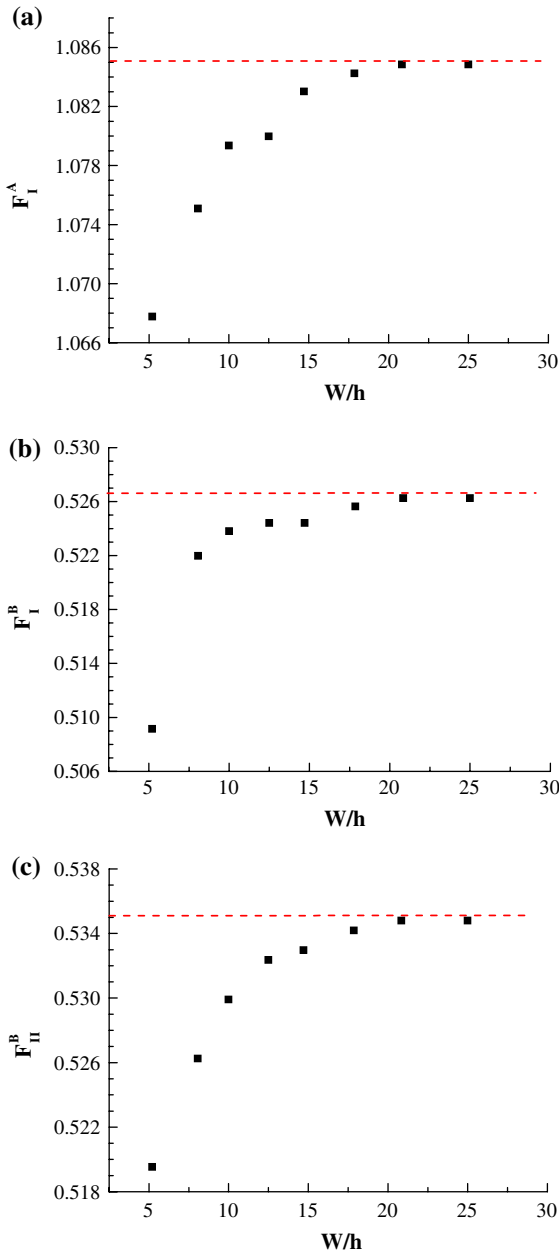


**Fig. 11** Variations of the normalized SIFs with the cover size for the branched crack problem. **a**  $F_I^A$ . **b**  $F_I^B$ . **c**  $F_{II}^B$  (dash line represents the converging value of each normalized SIF)

In this example, the plate dimensions are fixed to be  $W = 5$  and  $H = 4$ , and material constants are the Young's modulus  $E = 1000$  and the Poisson's ratio  $\nu = 0.3$ . The uniform tension at the boundary is assumed to be  $\sigma = 1.0$ . The normalized stress intensity factors for tips A and B are defined as

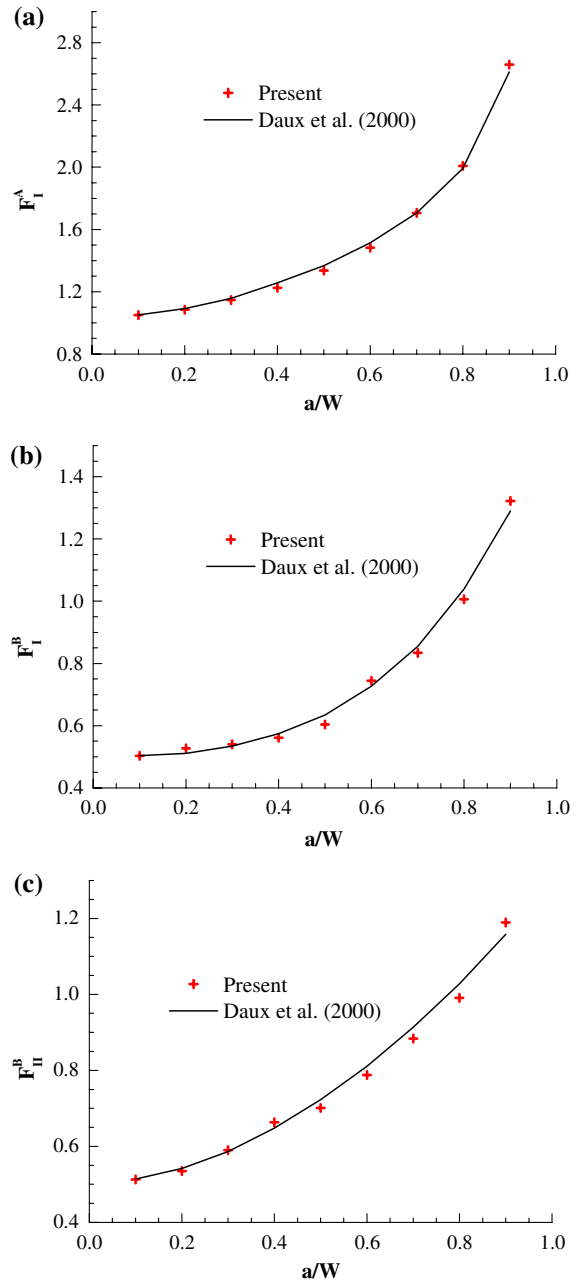


**Fig. 12** Comparison of the normalized SIFs for a branched crack problem. **a**  $F_I^A$ . **b**  $F_I^B$ . **c**  $F_{II}^B$

$$\begin{aligned}
 F_I^A &= K_I^A / \sigma \sqrt{\pi c}, & F_I^B &= K_I^B / \sigma \sqrt{\pi c}, \\
 F_{II}^B &= K_{II}^B / \sigma \sqrt{\pi c} & &
 \end{aligned}
 \tag{17}$$

with  $c = (a + b \cos \theta) / 2$  (see Fig. 9).

As previously mentioned in Sect. 2.2, the uniform hexagonal MCs like those in Fig. 2 are chosen, based

**Table 1** Normalized SIFs comparison for a branched crack

$b/a$	$\theta$	30°			45°			60°		
		NMM	*	RE (%)	NMM	*	RE (%)	NMM	*	RE (%)
0.1	$F_I^A$	1.020	1.008	1.19	0.999	1.010	1.09	1.002	1.012	0.99
	$F_I^B$	0.669	0.679	1.47	0.553	0.560	1.25	0.386	0.390	1.03
	$F_{II}^B$	0.196	0.199	1.51	0.352	0.347	1.44	0.430	0.435	1.15
0.3	$F_I^A$	1.022	1.016	0.59	1.026	1.019	0.69	1.020	1.023	0.29
	$F_I^B$	0.664	0.661	0.45	0.509	0.512	0.59	0.307	0.309	0.65
	$F_{II}^B$	0.274	0.276	0.72	0.441	0.438	0.68	0.521	0.526	0.95
0.5	$F_I^A$	1.013	1.021	0.78	1.016	1.026	0.97	1.026	1.033	0.68
	$F_I^B$	0.652	0.658	0.91	0.496	0.500	0.80	0.290	0.288	0.69
	$F_{II}^B$	0.311	0.309	0.65	0.470	0.474	0.84	0.563	0.559	0.72
0.7	$F_I^A$	1.027	1.024	0.29	1.036	1.033	0.29	1.038	1.046	0.76
	$F_I^B$	0.658	0.657	0.15	0.499	0.496	0.60	0.284	0.282	0.71
	$F_{II}^B$	0.324	0.327	0.92	0.497	0.493	0.81	0.577	0.573	0.70
0.9	$F_I^A$	1.034	1.028	0.58	1.042	1.040	0.19	1.054	1.061	0.66
	$F_I^B$	0.655	0.658	0.46	0.499	0.495	0.81	0.282	0.281	0.36
	$F_{II}^B$	0.396	0.399	0.75	0.507	0.503	0.80	0.580	0.577	0.52

\*Chen and Hasebe (1995)

on which PCs and CEs are formed. In addition, to manifest the resolution of the mathematical cover system, we define the cover size  $h$  as the radius of the circumscribed circle of MC cover in this context.

To study the convergence, a branched crack with  $a/W = b/W = 0.2$  and  $\theta = 45^\circ$  is investigated. The representative discretized domain with cover size  $h = 0.18W$  is shown in Fig. 10, in which there are 493 MCs, 503 PCs and 913 CEs. The SIFs for different cover size  $h$  are calculated and the normalized SIF results versus  $W/h$  are plotted in Fig. 11. It is evident that the SIF converges to a certain value as the MC is consecutively refined.

Next, the influence of the finiteness of plate on the SIFs is examined by varying  $a/W$  from 0.1 to 0.9 while keeping  $a/b = 1$ ,  $\theta = 45^\circ$  and  $h = 0.04W$ . The SIFs are calculated and compared with the reference solution from the XFEM (Daux et al. 2000) in Fig. 12. It is seen that the agreement between the present results and the reference solution is satisfactory.

The influence of the crack geometry on the SIFs is also investigated by varying  $b/a$  and  $\theta$ , while fixing  $a/W = 0.05$ . In calculation,  $h$  takes the value of  $0.02W$  for relatively larger  $b/a$  (e.g. 0.5, 0.7 and 0.9), while  $h = 0.01W$  for smaller  $b/a$  to assure that there is only one crack tip in a CE. Since the crack size is sufficiently small as compared with the plate size in our modeling, it is reasonable to choose the SIFs of a branched crack in an infinite plate as the reference solu-

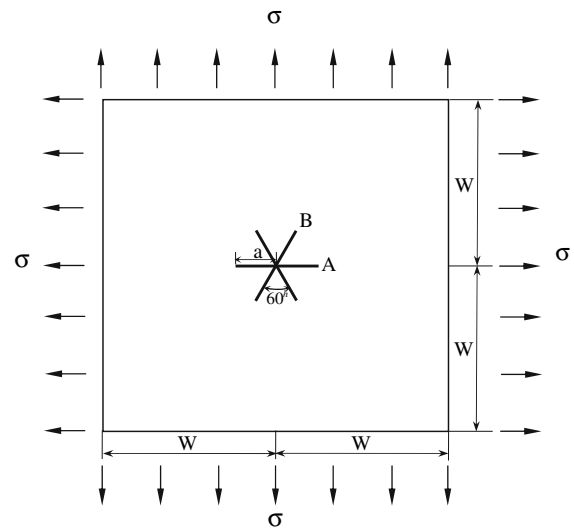


**Fig. 13** A star-shaped crack in a square plate under bi-axial tension

tion (Chen and Hasebe 1995). The SIF results from the present NMM and the reference solution (Chen and Hasebe 1995) are listed in Table 1. It is seen that the relative error (RE) is less than 1.6% for all the cases.

### 3.2 A star-shaped crack in a square plate

Next, we examine a star-shaped crack in a square plate subjected to bi-axial tension as shown in Fig. 13. The

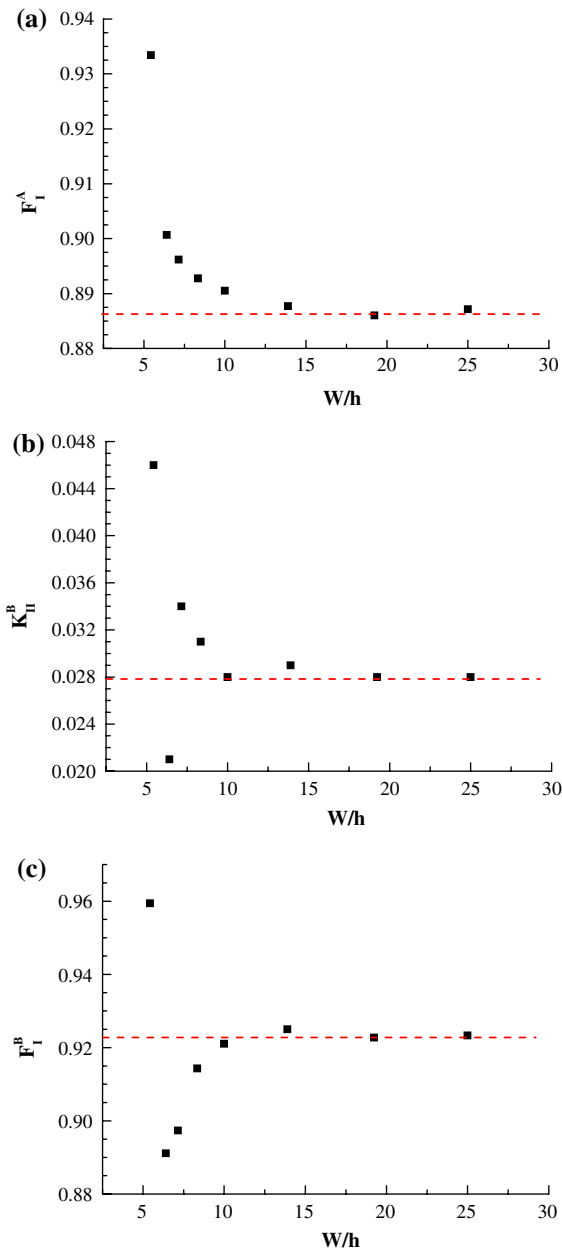


**Fig. 14** Variation of the SIFs with the cover size for a star-shaped crack problem. **a**  $F_I^A$ , **b**  $F_I^B$ . **c**  $F_{II}^B$  (dash line represents the converging value of each normalized SIF)

normalized stress intensity factors at tips A and B are defined as

$$\begin{aligned}
 F_I^A &= K_I^A / \sigma \sqrt{\pi a}, & F_I^B &= K_I^B / \sigma \sqrt{\pi a}, \\
 F_{II}^B &= K_{II}^B / \sigma \sqrt{\pi a}
 \end{aligned}
 \tag{18}$$

In the analysis, the plate size is taken to be  $W = 2.0$ , and the bi-axial tension to be unity. The normalized

**Table 2** Number of PCs and CEs for different  $a/W$

$a/W$	0.1	0.2	0.3	0.4	0.5	0.6	0.7	0.8	0.9
PCs	2921	2951	2979	3009	3037	3065	3095	3123	3153
CEs	5612	5642	5670	5700	5728	5756	5786	5814	5844

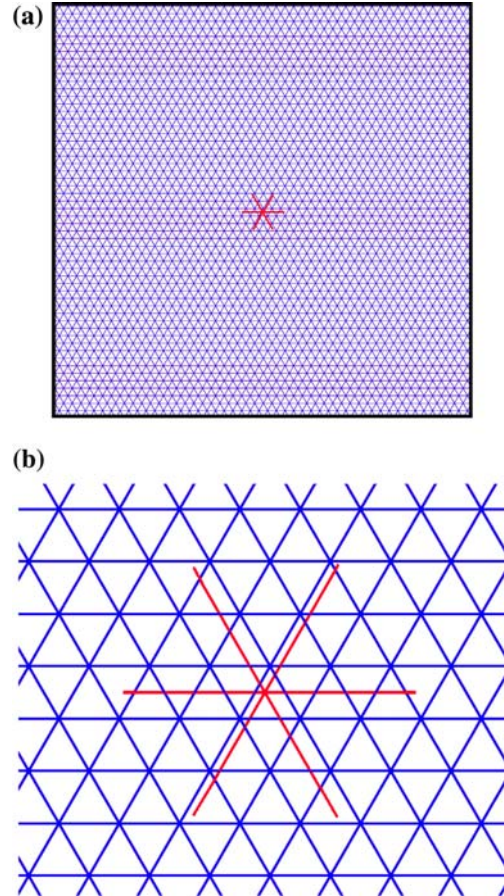


**Fig. 15** Star-shaped crack and MCs ( $a/W = 0.1$ ). **a** Global view. **b** Zoom in the region of the star-shaped crack

SIFs are inspected. The results for different cover sizes are plotted in Fig. 14 for the case of  $a/W = 0.2$ , and the convergence can be apparently found as the cover size is consecutively decreased.

Similar to that in Sect. 3.1, the influence of the finiteness of plate on the SIFs is also investigated. This time, the cover size  $h = 0.05W$  is used. In this case, the number of MCs is fixed at 2895, while numbers of PCs and CEs changes with the crack length (see Table 2). It should be noted that the numbers of MCs, PCs and CEs in this paper can be sharply decreased if adaptive finite element mesh is adopted. However, it is not the issue of the current study. To avoid the tediousness,

**Table 3** Normalized SIFs comparison for a star-shaped crack

$a/W$	$F_I^A$				$F_I^B$				$F_{II}^B$			
	NMM	*	**	***	NMM	*	**	***	NMM	*	**	***
0.1	0.758	0.751	–	0.741	0.767	0.769	–	0.741	0	0	–	0
0.2	0.771	0.767	0.769	0.757	0.771	0.768	0.769	0.758	0	0.001	0.001	0.001
0.3	0.789	0.793	0.797	0.785	0.798	0.798	0.799	0.788	0.002	0.002	0.002	0.002
0.4	0.821	0.829	0.835	0.826	0.854	0.847	0.853	0.837	0.007	0.008	0.008	0.007
0.5	0.887	0.886	0.892	0.885	0.924	0.926	0.923	0.909	0.016	0.018	0.02	0.017
0.6	0.971	0.967	0.975	0.976	1.04	1.045	1.041	1.018	0.036	0.036	0.045	0.034
0.7	1.107	1.097	1.102	1.114	1.234	1.237	1.238	1.194	0.061	0.059	0.062	0.053
0.8	1.340	1.342	1.345	–	1.559	1.562	1.558	–	0.082	0.086	0.08	–
0.9	1.930	1.931	1.915	–	2.166	2.193	2.161	–	0.089	0.087	0.091	–

\* Daux et al. (2000), \*\* Muravin and Turkel (2006), \*\*\* Cheung et al. (1984)  
 ‘–’, means no corresponding solution

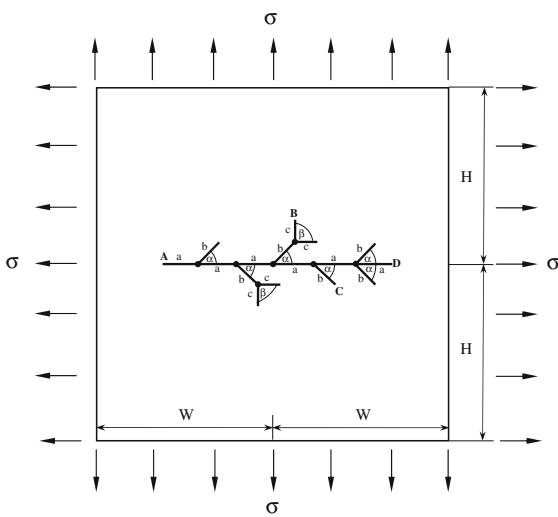


**Fig. 16** A tree-shaped crack in a square plate under bi-axial tension

only the CEs for the case of  $a/W = 0.1$  are shown in Fig. 15. The computed SIF results are summarized and compared with three reference solutions, respectively from Daux et al. (2000), Muravin and Turkel (2006), and Cheung et al. (1984) in Table 3. From this table, the excellent accuracy can also be easily seen.

### 3.3 A tree-shaped crack in a finite plate

The last example is intended to show the capability of the present NMM in solving very complex crack problems. As shown in Fig. 16, this is a coined problem with a tree-shaped crack under tension in a finite plate.

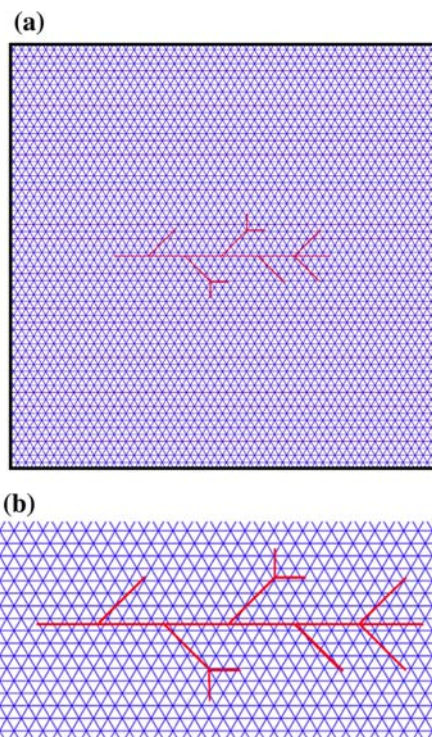
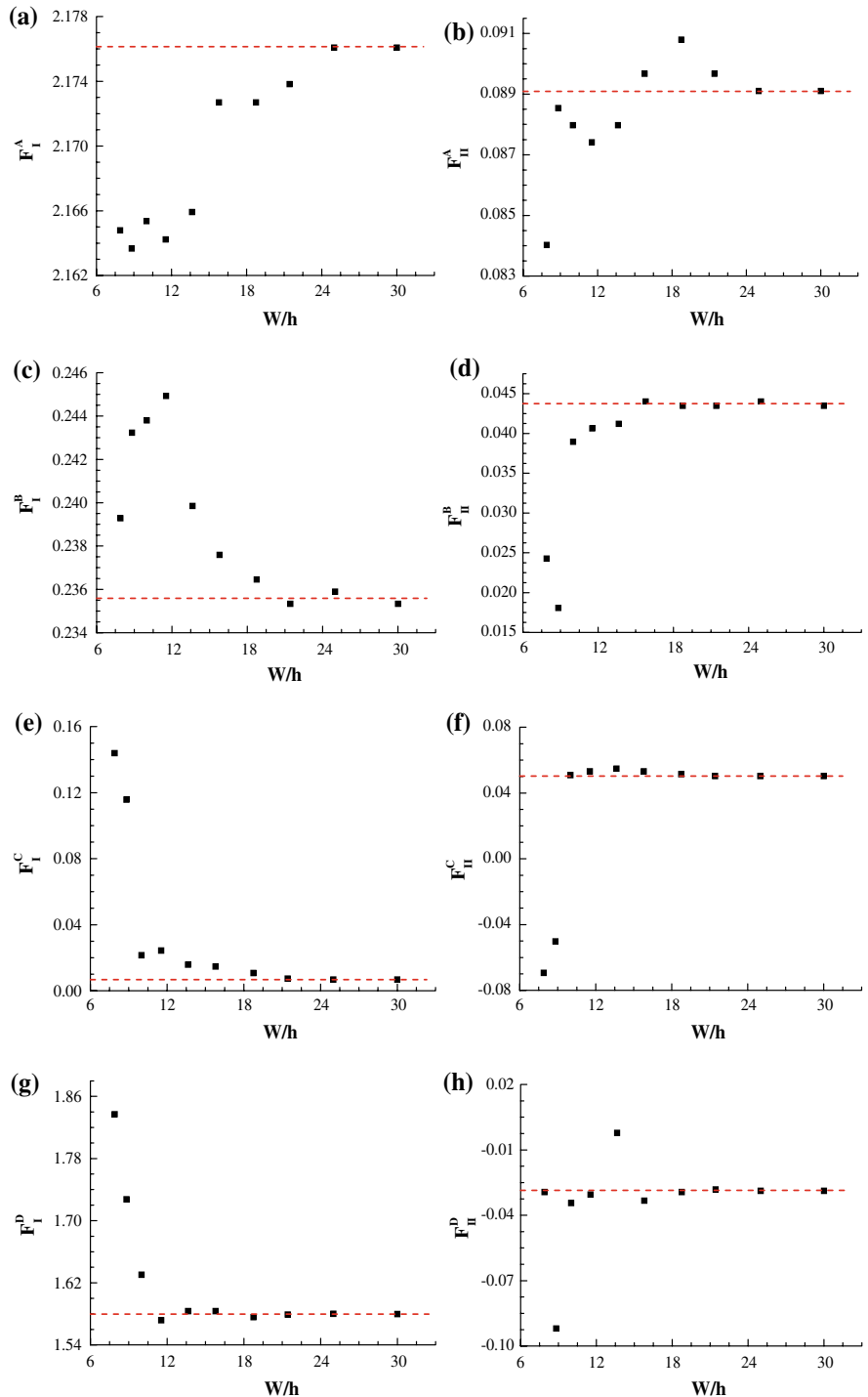


**Fig. 17** Tree-shaped crack and MCs. **a** The discretized domain with cover size  $h = 0.073 W$ . **b** Zoom in the region of tree-shaped crack

Solving this example seems very difficult by using the XFEM and GFEM. However, using the NMM, it can be treated in quite a same manner as in Sects. 3.1 and 3.2.

In computation, the dimensions are  $W = H = 6.0$ ,  $a = b = 2c = 1.0$  and  $\alpha = 45^\circ$ ,  $\beta = 90^\circ$ . The external load is bi-axial uniform tension with  $\sigma = 1.0$ .

**Fig. 18** Variation of the SIFs with the cover size for tree-shaped crack. **a**  $F_I^A$ , **b**  $F_{II}^B$ , **c**  $F_{II}^C$ , **d**  $F_{II}^D$ , **e**  $F_I^C$ , **f**  $F_{II}^C$ , **g**  $F_I^D$ , **h**  $F_{II}^D$  (dash line represents the converging value of each normalized SIF)



The material constants are  $E = 1000$  for the Young's modulus and  $\nu = 0.3$  for the Poisson's ratio.

To the authors' knowledge, the reference solution to this problem is not available. So, the current work

focuses on the convergence test for such a problem, and the crack tips labeled by A, B, C and D in Fig. 16 are investigated. The normalized SIFs for these crack tips are expressed as



$$F_I^M = K_I^M / \sigma \sqrt{\pi a}, \quad F_{II}^M = K_{II}^M / \sigma \sqrt{\pi a} \quad (M = A, B, C, D) \quad (19)$$

The calculation of SIFs for different cover sizes  $h$  is performed. For the case of  $h = 0.073 W$ , 3636 overlapping hexagonal MCs are used to cover the whole physical domain, and 3744 PCs together with 7125 CEs are eventually formed, as shown in Fig. 17. The SIFs results for different values of  $W/h$  are plotted in Fig. 18. It is seen that, even for such a complex problem, the NMM shows a consistent convergence as the MCs are gradually refined.

#### 4 Conclusions

The numerical manifold method was originally devised to solve discontinuous problems by introducing the concepts of mathematical cover and physical cover. It has two distinct features: one is that the mathematical covers are independent of the physical domain, and the other is that the DOFs are defined over the physical covers. In combination with the crack problems, the method was first summarized in detail, and the formulations were then derived. Three numerical experiments for complex crack problems such as a branched crack, a star-shaped crack and a coined tree-shaped crack problem were conducted. The results fully exhibited that with the numerical manifold method the complex crack problems can be effectively modeled in a more natural manner. The forthcoming work to model the growth of complex cracks with this method is now under study and the results are awaited. Together with the well known advantageous property in modeling blocky problems, the numerical manifold method so far seems to be a promising approach to tackle the whole failure process of material or a structure including crack initiation, crack growth, crack coalescence, and then formation of a complete failure plane, and lastly movement of discrete bodies.

#### References

- Babuska I, Melenk JM (1997) The partition of unity method. *Int J Numer Methods Eng* 40:727–758. doi:[10.1002/\(SICI\)1097-0207\(19970228\)40:4<727::AID-NME86>3.0.CO;2-N](https://doi.org/10.1002/(SICI)1097-0207(19970228)40:4<727::AID-NME86>3.0.CO;2-N)
- Barsoum R (1977) Triangular quarter-point elements as elastic and perfectly-plastic crack tip elements. *Int J Numer Methods Eng* 11:85–98. doi:[10.1002/nme.1620110109](https://doi.org/10.1002/nme.1620110109)
- Belytschko T, Tabbara M (1996) Dynamic fracture using element-free Galerkin methods. *Int J Numer Methods Eng* 39:923–938. doi:[10.1002/\(SICI\)1097-0207\(19960330\)39:6<923::AID-NME887>3.0.CO;2-W](https://doi.org/10.1002/(SICI)1097-0207(19960330)39:6<923::AID-NME887>3.0.CO;2-W)
- Belytschko T, Lu YY, Gu L (1994) Element-free Galerkin methods. *Int J Numer Methods Eng* 37:229–256. doi:[10.1002/nme.1620370205](https://doi.org/10.1002/nme.1620370205)
- Belytschko T, Lu YY, Gu L (1995a) Crack propagation by element-free Galerkin methods. *Eng Fract Mech* 51(2):295–315. doi:[10.1016/0013-7944\(94\)00153-9](https://doi.org/10.1016/0013-7944(94)00153-9)
- Belytschko T, Lu YY, Gu L, Tabbara M (1995b) Element-free Galerkin methods for static and dynamic fracture. *Int J Solids Struct* 32(17–18):2547–2570. doi:[10.1016/0020-7683\(94\)00282-2](https://doi.org/10.1016/0020-7683(94)00282-2)
- Belytschko T, Krongauz Y, Organ D, Fleming M, Krysl P (1996) Meshless methods: an overview and recent developments. *Comput Methods Appl Mech Eng* 139:3–47. doi:[10.1016/S0045-7825\(96\)01078-X](https://doi.org/10.1016/S0045-7825(96)01078-X)
- Chen Y, Hasebe N (1995) New integration scheme for the branch crack problem. *Eng Fract Mech* 52:791–801. doi:[10.1016/0013-7944\(95\)00052-W](https://doi.org/10.1016/0013-7944(95)00052-W)
- Chen GQ, Ohnishi Y, Ito T (1998) Development of high-order manifold method. *Int J Numer Methods Eng* 43:685–712. doi:[10.1002/\(SICI\)1097-0207\(19981030\)43:4<685::AID-NME442>3.0.CO;2-7](https://doi.org/10.1002/(SICI)1097-0207(19981030)43:4<685::AID-NME442>3.0.CO;2-7)
- Cheung Y, Wang Y, Woo C (1984) A general method for multiple crack problems in a finite plate. *Comput Mech* 20:583–589
- Chiou YJ, Lee YM, Tsay RJ (2002) Mixed mode fracture propagation by manifold method. *Int J Fract* 114:327–347. doi:[10.1023/A:1015713428989](https://doi.org/10.1023/A:1015713428989)
- Daux C, Moes N, Dolbow J, Sukumar N, Belytschko T (2000) Arbitrary branched and intersecting cracks with the extended finite element method. *Int J Numer Methods Eng* 48:1741–1760. doi:[10.1002/1097-0207\(20000830\)48:12<1741::AID-NME956>3.0.CO;2-L](https://doi.org/10.1002/1097-0207(20000830)48:12<1741::AID-NME956>3.0.CO;2-L)
- Duarte CA, Reno LG, Simone A (2007) A high-order generalized FEM for through-the thickness branched cracks. *Int J Numer Methods Eng* 72:325–351. doi:[10.1002/nme.2012](https://doi.org/10.1002/nme.2012)
- Dufflot M, Nauyen-Dang H (2004) A meshless method with enriched weight functions for fatigue crack growth. *Int J Numer Methods Eng* 59:1945–1961. doi:[10.1002/nme.948](https://doi.org/10.1002/nme.948)
- Fleming M, Chu YA, Moran B, Belytschko T (1997) Enriched element-free Galerkin methods for crack tip fields. *Int J Numer Methods Eng* 40:1483–1504. doi:[10.1002/\(SICI\)1097-0207\(19970430\)40:8<1483::AID-NME123>3.0.CO;2-6](https://doi.org/10.1002/(SICI)1097-0207(19970430)40:8<1483::AID-NME123>3.0.CO;2-6)
- Huang R, Sukumar N, Prevost JH (2003) Modeling quasi-static crack growth with the extended finite element method part II: numerical applications. *Int J Solids Struct* 40:7539–7552. doi:[10.1016/j.ijsolstr.2003.08.001](https://doi.org/10.1016/j.ijsolstr.2003.08.001)
- Karihaloo BL, Xiao QZ (2003) Modeling of stationary and growing cracks in FE framework without remeshing: a state-of-the-art review. *Comput Struct* 81:119–129. doi:[10.1016/S0045-7949\(02\)00431-5](https://doi.org/10.1016/S0045-7949(02)00431-5)
- Krysl P, Belytschko T (1999) Element-free Galerkin method for dynamic propagation of arbitrary 3-D cracks. *Int J Numer Methods Eng* 44:767–800. doi:[10.1002/\(SICI\)1097-0207\(19990228\)44:6<767::AID-NME524>3.0.CO;2-G](https://doi.org/10.1002/(SICI)1097-0207(19990228)44:6<767::AID-NME524>3.0.CO;2-G)

- Kwon YW, Akin JE (1989) Development of a derivative singular element for application to crack propagation problems. *Comput Struct* 31(3):467–471. doi:[10.1016/0045-7949\(89\)90394-5](https://doi.org/10.1016/0045-7949(89)90394-5)
- Li SC, Li SC, Cheng YM (2005) Enriched meshless manifold method for two-dimensional crack modeling. *Theor Appl Fract Mech* 44:234–248. doi:[10.1016/j.tafmec.2005.09.002](https://doi.org/10.1016/j.tafmec.2005.09.002)
- Lin JS (2003) A mesh-based partition of unity method for discontinuity modeling. *Comput Methods Appl Mech Eng* 192:1515–1532. doi:[10.1016/S0045-7825\(02\)00655-2](https://doi.org/10.1016/S0045-7825(02)00655-2)
- Melenk JM, Babuska I (1996) The partition of unity finite element method: basic theory and applications. *Comput Methods Appl Mech Eng* 139:289–314. doi:[10.1016/S0045-7825\(96\)01087-0](https://doi.org/10.1016/S0045-7825(96)01087-0)
- Moes N, Dolbow J, Belytschko T (1999) A finite element method for crack growth without remeshing. *Int J Numer Methods Eng* 46:131–150. doi:[10.1002/\(SICI\)1097-0207\(19990910\)46:1<131::AID-NME726>3.0.CO;2-J](https://doi.org/10.1002/(SICI)1097-0207(19990910)46:1<131::AID-NME726>3.0.CO;2-J)
- Muravin B, Turkel E (2006) Multiple crack weight for solution of multiple intersecting cracks by meshless numerical methods. *Int J Numer Methods Eng* 67:1146–1159. doi:[10.1002/nme.1661](https://doi.org/10.1002/nme.1661)
- Rao BN, Rahman S (2000) An efficient meshless method for fracture analysis of cracks. *Comput Mech* 26:398–408. doi:[10.1007/s004660000189](https://doi.org/10.1007/s004660000189)
- Shi GH (1991) Manifold method of material analysis. In: *Transactions of the 9th army conference on applied mathematics and computing*, Minneapolis, Minnesota, pp 57–76
- Shi GH (1992) Modeling rock joints and blocks by manifold method. In: *Proceedings of the 33rd US rock mechanics symposium*, Santa Fe, New Mexico, pp 639–648
- Simone A, Duarte CA, Van Der Giessen E (2006) A generalized finite element method for polycrystals with discontinuous grain boundaries. *Int J Numer Methods Eng* 67:1122–1145. doi:[10.1002/nme.1658](https://doi.org/10.1002/nme.1658)
- Strouboulis T, Babuska I, Copps K (2000a) The design and analysis of the generalized finite element method. *Comput Methods Appl Mech Eng* 181:43–69. doi:[10.1016/S0045-7825\(99\)00072-9](https://doi.org/10.1016/S0045-7825(99)00072-9)
- Strouboulis T, Copps K, Babuska I (2000b) The generalized finite element method: an example of its implementation and illustration of its performance. *Int J Numer Methods Eng* 47:1401–1417. doi:[10.1002/\(SICI\)1097-0207\(20000320\)47:8<1401::AID-NME835>3.0.CO;2-8](https://doi.org/10.1002/(SICI)1097-0207(20000320)47:8<1401::AID-NME835>3.0.CO;2-8)
- Strouboulis T, Copps K, Babuska I (2001) The generalized finite element method. *Comput Methods Appl Mech Eng* 190:4081–4193. doi:[10.1016/S0045-7825\(01\)00188-8](https://doi.org/10.1016/S0045-7825(01)00188-8)
- Sukumar N, Prevost JH (2003) Modeling quasi-static crack growth with the extended finite element method part I: computer implementation. *Int J Solids Struct* 40:7513–7537. doi:[10.1016/j.jjsolstr.2003.08.002](https://doi.org/10.1016/j.jjsolstr.2003.08.002)
- Sukumar N, Moes N, Moran B, Belytschko T (2000) Extended finite element method for three-dimensional crack modeling. *Int J Numer Methods Eng* 48:1549–1570. doi:[10.1002/1097-0207\(20000820\)48:11<1549::AID-NME955>3.0.CO;2-A](https://doi.org/10.1002/1097-0207(20000820)48:11<1549::AID-NME955>3.0.CO;2-A)
- Tsay RJ, Chiou YJ, Chuang WL (1999) Crack growth prediction by manifold method. *J Eng Mech* 125:884–890. doi:[10.1061/\(ASCE\)0733-9399\(1999\)125:8\(884\)](https://doi.org/10.1061/(ASCE)0733-9399(1999)125:8(884))